J Solid State Electrochem (2009) 13:1051–1061
DOI 10.1007/s10008-008-0685-1

REVIEW

The application of synchrotron techniques to the study of lithium-ion batteries

James McBreen

Received: 24 July 2008 / Revised: 17 September 2008 / Accepted: 19 September 2008 / Published online: 9 October 2008

Abstract This paper gives a brief review of the application of synchrotron X-ray techniques to the study of lithium-ion battery materials. The two main techniques are X-ray absorption spectroscopy (XAS) and high-resolution X-ray diffraction (XRD). Examples are given for in situ XAS and XRD studies of lithium-ion battery cathodes during cycling. This includes time-resolved methods. The paper also discusses the application of soft X-ray XAS to do ex situ studies on battery cathodes. By applying two signal detection methods, it is possible to probe the surface and the bulk of cathode materials simultaneously. Another example is the use of time-resolved XRD studies of the decomposition of reactions of charged cathodes at elevated temperatures. Measurements were done both in the dry state and in the presence of electrolyte. Brief reports are also given on two new synchrotron techniques. One is inelastic X-ray scattering, and the other is synchrotron X-ray reflectometry studies of the surface electrode interface (SEI) on highly oriented single crystal lithium battery cathode surfaces.

X-ray absorption spectroscopy

When I joined John Bockris' Group in October 1961, almost all of the electrode studies were electrical measurements. A few months later, the Group bought an ellipsometer. This instrument gave many insights into the structure of surface films. Ellipsometry is an in situ technique that can be used to study film growth on electrodes. The advantage of ellipsometry is that it is an in situ technique that can be used to study film growth on electrodes. The main disadvantage is that it does not provide chemical information. Later on, Bockris and Habib had major success in applying Fourier Transform Raman spectroscopy to in situ studies [1]. The great advantage was the ability to get chemical information.

The application of X-ray absorption spectroscopy (XAS) to structural determinations is a relatively new technique. The acquisition of good XAS spectra requires an X-ray source with a brightness that is at least six orders of magnitude higher than that delivered by a rotating anode source. Until 1971, there was no acceptable theory for extended X-ray absorption fine structure (EXAFS). Thus, there was no incentive to build synchrotron X-ray sources. In 1971, Sayers et al. made a major advance in the theory [2]. They found that short-range structural data could be obtained from Fourier analysis of the EXAFS. This led to the construction of dedicated storage rings, beginning at Daresbury, England in 1981. This was quickly followed by the construction of the National Synchrotron Light Source (NSLS) at Brookhaven National Laboratory (BNL) and the LURE facility in Orsay, France. Today, there are a total of 45 synchrotron facilities worldwide. About half of them are located in Japan, USA, and Germany. The rest are located in 16 other countries, including Australia, Brazil, Canada, China, Denmark, France, India, Italy, Korea, Russia, Singapore, Spain, Sweden, Switzerland, Taiwan, and UK.

XAS is simply the accurate determination of the X-ray absorption coefficient of a material as a function of photon energy in an energy range that is below and above the absorption edge of one of the elements in the material. In the case of lithium-ion battery materials, absorption measurements are usually done a K edge. The K edge is due to absorption by 1s core states. Measurements at the K

Dedicated to the 85th birthday of John O'M. Bockris

J. McBreen (✉)
Department of Condensed Matter Physics and Materials Science,
Brookhaven National Laboratory,
Upton, NY 11973, USA
e-mail: jmcbreen@bnl.gov

edge are most suitable for elements of low atomic number (low Z) and for first row transition metal elements. With the advent of XAS, extensive research on the electronic structure of Li-ion-intercalated cathode materials has been carried out to elucidate the reaction mechanism of the electrochemical process in the cathode material during cycling. In situ hard XAS has been employed in to examine the electronic and local structure of transition metal ions in cathode in Li rechargeable batteries. The absorption peak features of the transition metal K-edge XAS provide useful structural information such as the oxidation state of chemical species, their site symmetries, and covalent bond strength.

Soft X-ray XAS is an ex situ technique that uses soft X-rays, with energies in the range of 150–1,200 eV to do XAS. This energy range covers the K edges of B, C, N, O, and F and the $L_{2,3}$ edges of the first row transition metal elements. Soft X-ray XAS has some degree of surface specificity. In an XAS, experiment tuneable X-rays impinge on a sample. When the X-ray reaches a specific energy, such as the K edge of oxygen (532 eV), 1s electrons are ejected. The resultant core hole can relax in two ways: One is by having an electron drop from higher levels into the core hole. This results in the emission of fluorescent X-rays. The other mode of relaxation is the ejection of Auger electrons. A schematic diagram of the process is given in Fig. 1. Both the fluorescent X-rays and the Auger electron signals are proportional to the X-ray absorption. So both signals can be processed to yield XAS spectra. The fluorescent X-rays have an escape depth of about 3,000 Å, whereas the Auger electrons have an escape depth of only 50 Å. So, the fluorescent X-ray signal gives information about the bulk and the Auger signal yields information on the region close to the surface. By simultaneously doing fluorescence and electron yield measurements, one can get both surface and bulk information in the same experiment.

Soft X-ray absorption measurements are done at low-energy synchrotron X-ray facilities such as the UV ring at NSLS or the Advanced Photon Source (APS) at Lawrence Berkeley National Laboratory (LBNL). The beam size is typically 1 mm in diameter. The electron yield data is usually obtained in the total electron yield (EY) mode, measuring the current from a channel electron multiplier (Channeltron). Sometimes, a voltage bias is applied to increase surface sensitivity. This is referred to as the partial electron yield mode. Fluorescence yield (FY) data are recorded using a windowless energy dispersive Si (Li) detector. The experiments are conducted in vacuum at a pressure of $\sim 2\times10^{-7}$ torr.

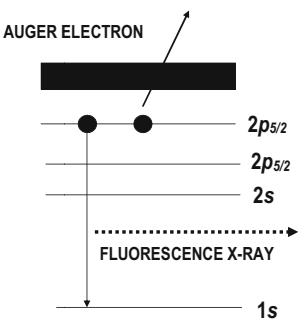

Fig. 1 Soft X-ray XAS. The *black band* represents states in the vicinity of the Fermi level

The most common first row elements in lithium-ion cathode materials are V, Cr, Mn, Fe, Co, Ni, and Cu. All of these can be easily probed in in situ experiments in the transmission mode. The energy range required ranges form 4.5 to 10 keV. Figure 2 is a schematic representation of the experimental configuration. It consists of an X-ray source, a double-crystal monochromator, a thin sample of the material, ionization chamber detectors for monitoring the beam intensity before, and after it passes through the material, and a data acquisition system. The data acquisition system is used for several purposes. This includes stepping the monochromator to pass the desired photon energies, alignment of the sample in the beam, and monitoring the signals from the detectors. Usually three detectors are used, with a reference sample such as a metal foil in front of the third detector. The time for obtaining a full spectrum is typically 20 min and is mainly limited by the dead time needed for rotation of the crystals in the monochromator.

During an XAS experiment, core electrons are excited. This produces empty states called core holes. These can relax by having electrons from outer shells drop into the core holes. This produces fluorescent X-rays that have a somewhat lower energy than the incident X-rays. The fluorescent signal is proportional to the absorption. Detection of this signal is a useful method for measuring absorption by dilute systems such as minor additives.

XAS is an ideal method for in situ studies of electrochemical systems, because both the probe and signal are penetrating X-rays. The great advantage is that XAS is element specific, and this permits investigation of the chemical environment of a constituent element in a composite material. It also permits studies of dilute systems. Since XAS probes only short-range order, it can provide structural information on amorphous materials, liquids, gases, adsorbed monolayers, as well as hydrated ions and complexes in solution. Because of its versatility, XAS is finding applications in an enormous variety of electrochemical systems, including battery electrode materials, and additives in battery electrodes.

Charge compensation mechanism during electrochemical Li-ion deintercalation of $Li_{1-x}Co_{1/3}Ni_{1/3}Mn_{1/3}O_2$

Hard XAS measurements were performed in transmission mode at beamline X18B of the NSLS using a Si(111) double-crystal monochromator detuned to 35–45% of its

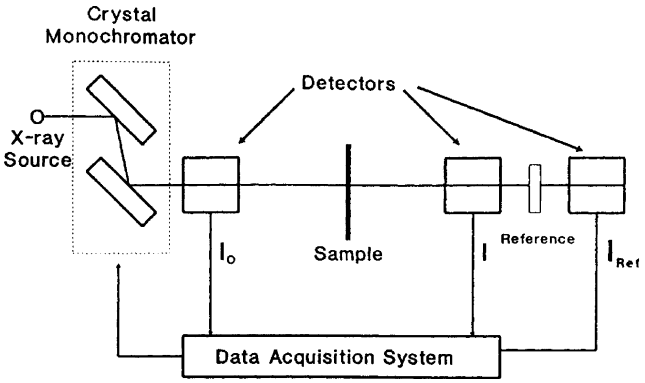

Fig. 2 Experimental setup for a transmission XAS experiment

original intensity to eliminate the high order harmonics. The in situ Mn, Co, and Ni K-edge XAS data were obtained in two separate cells. The Mn XAS spectra were collected using one cell, while the Co and Ni XAS spectra were collected in tandem using the second cell. Energy calibration was carried out by using the first inflection point of the spectrum of Mn and Ni metal foil as a reference (i.e., Mn K edge=6,539 eV and Ni K edge=8,333 eV). Reference spectra were simultaneously collected for each in situ spectrum by using Mn or Ni metal foils [3, 4].

Normalized Mn, Ni, and Co K-edge X-ray absorption near-edge structure (XANES) spectra of $Li_{1-x}Co_{1/3}Ni_{1/3}Mn_{1/3}O_2$ electrode during charge are shown in Fig. 3. The onset of the metal K-edge XANES spectra is due to symmetry-allowed transitions from the 1s core electron of the metal to excited vacant bound states. The weak pre-edge absorption is the formally electric dipole-forbidden transition of a 1s electron to an unoccupied 3d orbital, which gains peak intensity from pure electric quadrupole coupling and/or 3d–4p orbital mixing arising from the noncentrosymmetric environment of the slightly distorted octahedral 3a site in the rhombohedral *R*3*m* space group. The first strong absorption edge features occurring as a shoulder on the lower-energy region with respect to the main absorption edge are assigned to a shakedown process involving the 1s→4p transition followed by ligand-to-metal charge transfer. The main absorption edge features are ascribed to the purely dipole-allowed 1s→4p transition. As the Li-ion is deintercalated, the Mn XANES spectrum exhibits some changes in the shape of the edge due to changes in the Mn local environment but does not show a rigid shift to higher energy values. The energy position and the shape of these edges are very similar to those of the $Li_{1.2}Cr_{0.4}Mn_{0.4}O_2$ and $LiNi_{0.5}Mn_{0.5}O_2$ electrode materials, in which manganese remains as Mn^{4+} throughout charge [5, 6]. This provides clear evidence that most of Mn ions in pristine $Li_xCo_{1/3}Ni_{1/3}Mn_{1/3}O_2$ are already in the Mn^{4+} oxidation state and are not oxidized as a result of the Li deintercalation. Unlike the Mn K-edge XANES spectra, the Ni K-edge XANES spectra shift to higher energies during charge. The

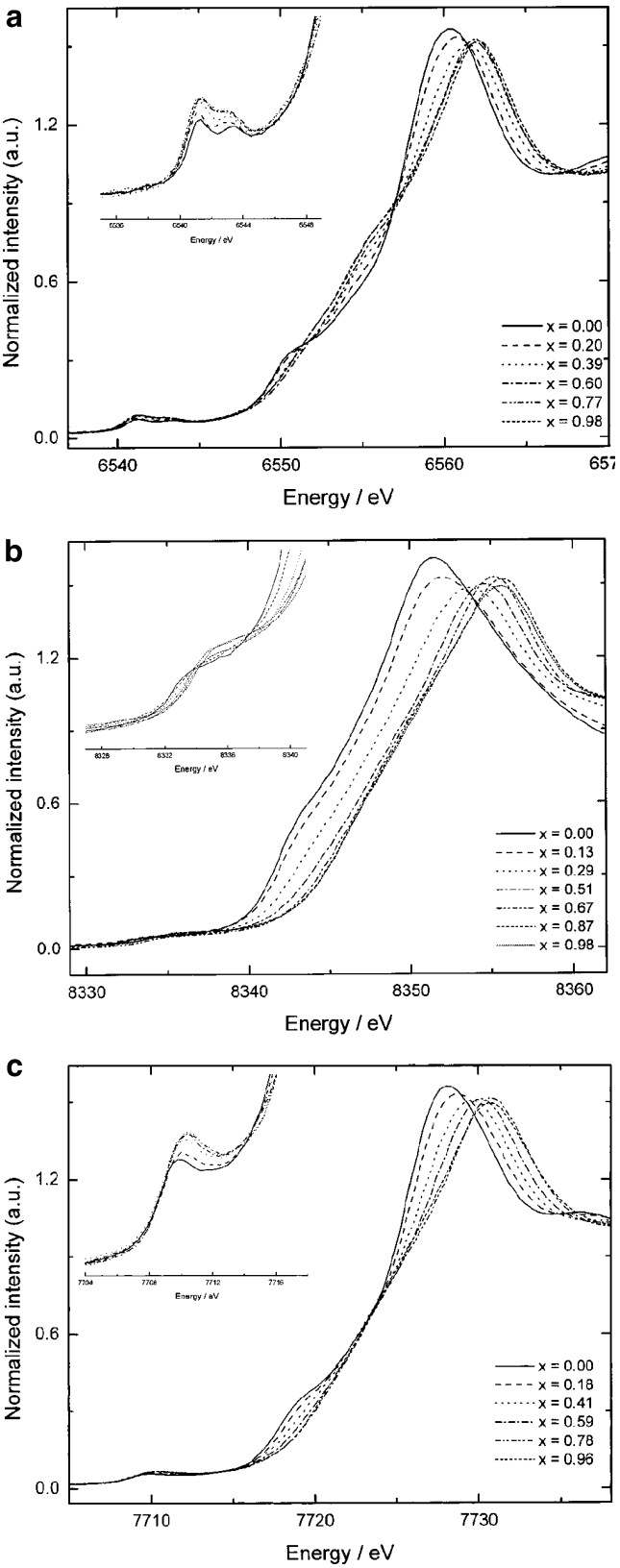

Fig. 3 Normalized **a** Mn, **b** Ni, and **c** Co K-edge XANES spectra of $Li_{1-x}Co_{1/3}Ni_{1/3}Mn_{1/3}O_2$ electrode during charge

entire edge shift to the higher energies indicates that the average oxidation state of nickel ions increases during charge. In the normal operating voltage (up to ~4.6 V) of this cathode, therefore, the charge compensation at metal site during Li deintercalation is achieved mainly by the oxidation of Ni^{2+} to Ni^{4+} ions. In the normal operating voltage (up to ~4.6 V) of this cathode, therefore, the charge compensation at metal site during Li deintercalation is achieved mainly by the oxidation of Ni^{2+} to Ni^{4+} ions.

The interpretation of Co K-edge spectra is more complicated in this system. The Co K-edge XAS spectra do not show a rigid edge shift during charge. In the case of the Co K-edge XAS results, changes in the edge shape during charge could be ascribed to the changes in bond length and covalency. The features of the charging curve indicate that there is further Li-ion deintercalation above 4.6 V. However, above 4.6 V, none of the three K edges displays any indication of a further rigid edge shift. Ten years ago, Ceder et al. reported based on theoretical calculations that electron exchange in cathode materials (i.e., oxidation and reduction) may involve the participation of oxygen 2p band, in addition to charge compensation by the metal ions [7]. Earlier soft XAS (200–1,000 eV) results from Yoon et al. at the O K edge have provided experimental evidence for this oxygen contribution to charge compensation in the Li-ion intercalation–deintercalation process [8].

The pre-edge peak positions and intensities in the ligand K-edge XAS spectra provide important structural information about the chemical bonding between ligand and metal atoms. The O K-edge XAS of electrochemically Li-ion deintercalated $Li_{1-x}Co_{1/3}Ni_{1/3}Mn_{1/3}O_2$ system is shown in Fig. 4. Pre-edge peaks below ~534 eV of these spectra correspond to the transition of oxygen 1s electron to the hybridized state of the transition metal 3d and oxygen 2p orbitals, whereas the broad higher peaks above ~534 eV correspond to the transitions to hybridized states of oxygen 2p and transition metal 4sp orbitals. Two major changes caused by the Li-ion deintercalation in the spectral features were observed in the pre-edge region: a shift of pre-edge peak position to the lower energy and an increase of the integrated pre-edge intensity. The shift to low energy is attributed to the higher oxidation state of metal ions due to the Li-ion deintercalation. The greater effective nuclear charge of the higher oxidation state metal ions shifts the ligand pre-edge peak position to lower energy, since the metal d orbitals are located at a deeper binding energy and are closer in energy to the ligand 1s orbital. We shall now focus on the second major change. The variation of the integrated pre-edge peak intensity with the electrochemical deintercalation can give important information about the hole state distribution and the effective charge on the oxygen atom, since the density of the empty bound state in the molecular energy level is related to the hybridization of

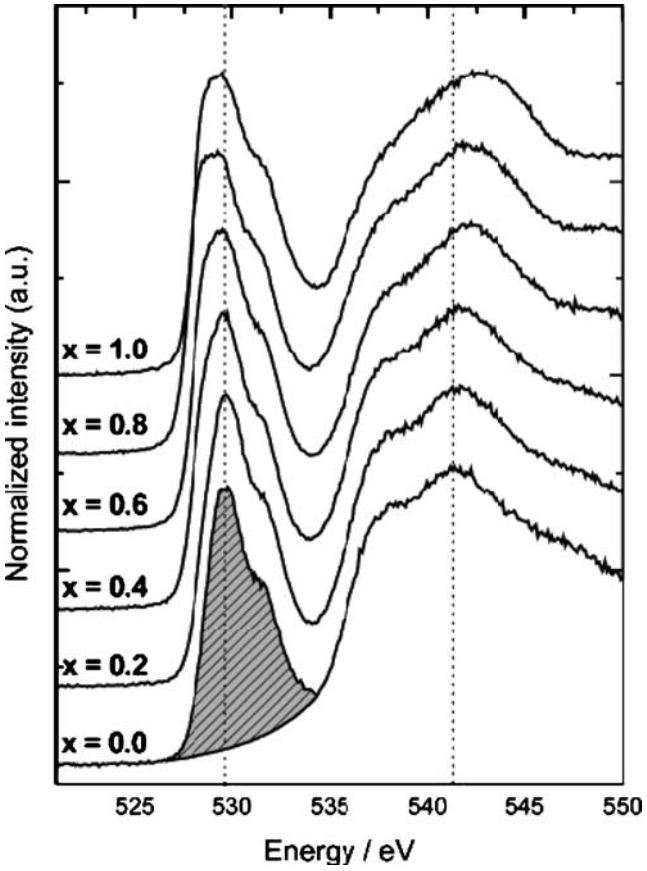

Fig. 4 The O K-edge XAS spectra in FY mode for electrochemically Li-ion deintercalated $Li_{1-x}Co_{1/3}Ni_{1/3}Mn_{1/3}O_2$ electrode during charge

metal 3d–O 2p orbitals. The shaded area in Fig. 4 is the integrated pre-edge intensity assigned to oxygen p character hybridized with the transition metal 3d band. The pre-edge peak intensity continuously increases in the range of $0 \le x \le 2/3$ in $Li_{1-x}Co_{1/3}Ni_{1/3}Mn_{1/3}O_2$. The spectral weight increases by ~37% from $x=0$ to 0.7 in $Li_{1-x}Co_{1/3}Ni_{1/3}Mn_{1/3}O_2$ compared to that of pristine $Li_{1-x}Co_{1/3}Ni_{1/3}Mn_{1/3}O_2$, indicating that a large portion of the holes that compensate the lithium-ion deintercalation are located in O 2p states. In contrast, our previous O K-edge results of the $Li_{1-x}Ni_{0.5}Mn_{0.5}O_2$ system showed relatively small change (~10% for $x=0$–0.8 in $Li_{1-x}Ni_{0.5}Mn_{0.5}O_2$) in the pre-edge intensity during charge [9]. $LiNi_{0.5}Mn_{0.5}O_2$ and $LiCo_{1/3}Ni_{1/3}Mn_{1/3}O_2$ can be considered as a member of $Li[Ni_xCo_{1-2x}Mn_x]O_2$ series. The major difference between $LiNi_{0.5}Mn_{0.5}O_2$ and $LiCo_{1/3}Ni_{1/3}Mn_{1/3}O_2$ systems is that the latter contains Co. Therefore, the increased pre-edge peak intensity observed is clearly due to the content of Co. In considering the contribution of Ni–O covalency, since the Ni content is higher in $Li_{1-x}Ni_{0.5}Mn_{0.5}O_2$ than in $Li_{1-x}Co_{1/3}Ni_{1/3}Mn_{1/3}O_2$, it would have had a larger weight of the pre-edge peak in the former one if the Ni–O covalency is the major contributor. On the basis of the fact that the larger weight of the pre-edge peak was observed in $Li_{1-x}Co_{1/3}Ni_{1/3}Mn_{1/3}O_2$, it is reasonable to believe that a

large portion of the charge compensation during Li-ion deintercalation appears to be achieved on oxygen sites, which are associated with Co.

The combination of soft and hard X-ray XAS and EXAFS probes proved to be a very powerful technique for elucidating the charge compensation mechanism for $Li_{1-x}Co_{1/3}Ni_{1/3}Mn_{1/3}O_2$.

P K-edge XAS studies of electrochemically delithiated $Li_{1-x}FePO_4$

A great deal of research on cathode materials has been carried out to identify an alternative nontoxic cathode material with higher capacity, lower cost, and increased safety to replace $LiCoO_2$. $LiFePO_4$ has recently been shown to be one of the most promising alternative materials for $LiCoO_2$, because its electrochemical and safety characteristics are better than $LiCoO_2$. These $LiFePO_4$ materials crystallize in an olivine structure containing Li in a framework composed of PO_4 tetrahedra and distorted FeO_6 octahedra. The use of (PO_4^{3-}) polyanion with a strong P–O covalent bond in the olivine LiFePO4 structure has been shown not only to lower the Fermi level of the Fe^{3+}/Fe^{2+} redox couple to useful levels (~3.5 V) but also to improve thermal stability of Li batteries. Phosphorus plays a critical role in the performance of the $LiFePO_4$ electrode. This is a summary of the first P K-edge XAS study on the electrochemically delithiated $Li_{1-x}FePO_4$ for Li rechargeable batteries [10].

Electrode specimens were prepared by mixing carbon-coated $LiFePO_4$ powders (Phostech, Canada) with 10 wt.% acetylene black and 10 wt.% polyvinylidene fluoride (PVDF) in *n*-methyl pyrrolidone solution. One molar $LiPF_6$ in a 1:1 ethyl carbonate/dimethyl carbonate (EC/DMC) solution was used as the electrolyte. The cell was assembled in an argon-filled glove box. The cells were first charged to the desired values of Li-ion content (x value) at a C/50 rate and then relaxed for a day. The electrochemical cells were disassembled in an argon-filled glove box, and the $LiFePO_4$ electrodes were taken out from the cell. The electrodes were then washed with tetrahydrofuran (THF) and dried thoroughly in vacuum.

The P K-edge XAS data collection was done at the NSLS using the Beamline X19A equipped with a Si(111) monochromator. The XAS data were collected in fluorescence mode at ambient temperature and pressure, under He, using a solid-state passivated implanted planar silicon detector.

The K-edge XANES absorbs element to excited vacant states of proper symmetry involving the element orbitals. Figure 5 shows normalized P K-edge XANES spectra of $Li_{1-x}FePO_4$ electrode as a function of x. The main edge peak at ~2,152.5 eV can be assigned to a transition of the

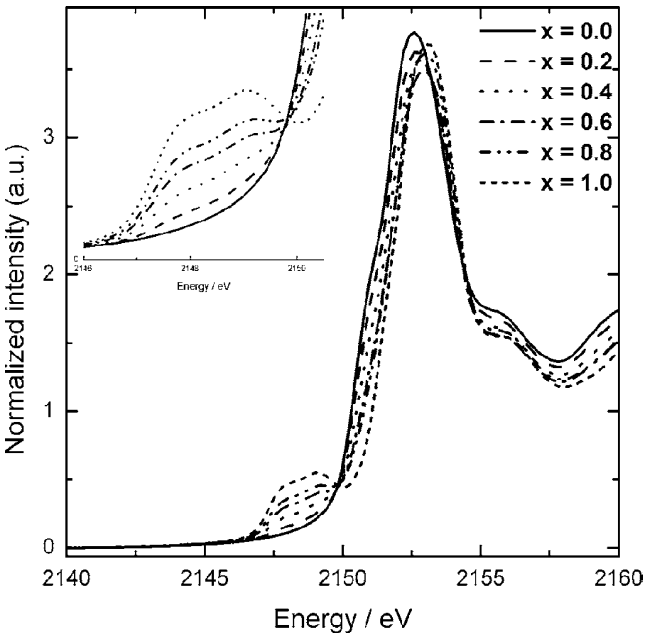

Fig. 5 Normalized P K-edge XANES spectra of $Li_{1-x}FePO_4$ electrode as a function of x

P 1s electron into an unoccupied valence electronic state formed by the overlap of Psp^3 hybrid- and O 2p-orbitals, because the PO_4 group has T_d-symmetry. The white line gradually moves towards the higher energy side as Li is extracted. The major charge compensation of $LiFePO_4$ during Li extraction is achieved by the oxidation of Fe^{2+} ions to Fe^{3+} ions, resulting in more covalent Fe–O bonds. In the olivine $LiFePO_4$ structure, polarization of the electrons of the oxygen ions towards the phosphorus ion reduces the covalent bonding to the iron ion by the inductive effect. Likewise, the increase in more covalent Fe^{3+}–O bonds makes the P–O bonds less covalent by the same inductive effect. A shift of the white line to the higher energy side reflects a change in the degree of covalency of the P–O bond altered by the presence of the more covalent Fe^{3+}–O bond during charge.

Surprisingly, chemical changes beyond the first coordination sphere around the phosphorus atoms have a systematic influence on the observed XANES spectrum. No pre-edge peak was observed in P K-edge XANES spectrum for the pristine $LiFePO_4$. Upon Li deintercalation, however, pre-edge peaks start to appear in the lower-energy region of the main edge. The pre-edge features of P K-edge XAS in transition metal phosphates reflects the interaction between metal 3d and P 3p states through the shared oxygen atom. The gradual increase of pre-edge peak intensities with the Li-ion extraction shows that these pre-edge peaks are due to the hybridization of P 3p states with the Fe 3d states, because this is consistent with the gradual increase in oxidation state of Fe ions with the Li-ion extraction. The P K-edge XANES spectrum originates from

the transition of a P 1s electron to an empty antibonding state of the anion. In $LiFePO_4$, this state must lie above the Fe^{3+}/Fe^{2+} redox couple. However, in the mixed-valent system, the empty states (Fe^{3+} ions) of this couple lie above the occupied states (Fe^{2+} ions), and the energy difference is amplified by the first-order change of volume. Therefore, one can imagine that the energies of the empty states of the Fe^{3+}/Fe^{2+} couple may overlap the empty antibonding states of the anions, in which case mixing of the minority-spin states of the Fe^{3+} ions and the antibonding states of the anions would occur. With a two-phase system, the volume fraction in which this interaction occurs would increase smoothly with the concentration of Fe^{3+} ions. Such hybridization between P 3p and Fe 3d states occurs in spite of the presence of oxygen atoms that separate phosphorus from iron. Consequently, the electronic structure of orthophosphates cannot be regarded rigorously as composed of traditional ion pairs for $(Li^{+})(Fe^{2+})$–(PO_4^{3-}) and (Fe^{3+})–(PO_4^{3-}), which are charged according to their formal valence.

Principal component analysis of the XANES spectra reveals that this set of spectra can be well represented by two primary components, in good agreement with a first-order phase transition involving the $LiFePO_4$ and $FePO_4$ phases.

In summary, P K-edge XAS has been carried out to investigate the electronic structure of the electrochemically delithiated $Li_{1-x}FePO_4$ for Li rechargeable batteries. The gradual shift of the main edge features to the higher energy side showed that P–O bonds become less covalent during delithiation due to the more covalent Fe^{3+}–O bonds via the inductive effect. From the observation of pre-edge peaks, it is concluded that electrochemical delithiation of $Li_{1-x}FePO_4$ results in the hybridization of P 3p states with the Fe 3d states.

The use of time-resolved synchrotron XRD to study the thermal decomposition of nickel-based layered cathode materials

Problems of power fade and safety concerns in high power lithium-ion cells are the major technical barriers that have to be overcome in order to meet the challenging requirement for hybrid electric vehicles applications. Safety characteristics are related to the occurrence of exothermic reactions in charged batteries at elevated temperatures that ultimately results in thermal runaway and catastrophic failure of the battery. The thermal runaway has been attributed to the reactions between the charged electrodes and the electrolyte. Temperature-dependent X-ray diffraction studies have provided useful information about these reactions. Unfortunately, most of the temperature-dependent diffraction studies of the structure of the charged electrodes have been performed in the absence of electrolyte/solvents. In order to understand thermal degradation of the electrodes in Li-ion cells, it is very important to monitor the structural changes of the charged cathode material in the presence of electrolyte. At BNL, we have developed a technique using the combination of a high intensity synchrotron X-ray beam and a fast-image plate detector to do time-resolved X-ray diffraction during the thermal decomposition of charged cathode materials in the presence of electrolyte [11].

Cathodes were supplied by Quallion (Sylmar, CA, USA). The cathode consists of 84% $LiNi_{0.8}Co_{0.15}Al_{0.05}O_2$ (Fuji Chemical), 4% carbon black (Chevron), 4% SFG-6 (Timical), and 8% PVDF (Kureha) on aluminum foil. The cathodes were incorporated into cells with a Li foil anode, a Celgard separator, and a 1 M $LiPF_6$ electrolyte in a 1:1 ethylene carbonate/dimethyl carbonate (EC/DMC) solvent (LP 30 from EM Industries). The cells were assembled in an argon-filled glove box and were hermetically sealed in a housing that could be easily disassembled. The cells were charged to various stages of charge outside the glove box. The cells were then transferred to the glove box for disassembly and transfer of charged cathode materials to quartz capillaries. Some of the charged cathode samples washed in THF in the glove box and were sealed in either 0.3 or 0.5 mm quartz capillaries. Other samples were not washed before loading the capillaries and wetted with a drop of excess electrolyte before sealing. These capillaries could withstand the pressure generated on heating. To simulate the real operating condition, excess electrolyte was added to the capillary to compensate the lost electrolyte during the disassembling of the cell. The capillaries were mounted in the thermal stage of diffractometers on beamline X7B, at NSLS at BNL, and XRD spectra were recorded as a set of circles on a Mar 345-image plate detector in the transmission mode. A complete XRD spectrum was taken on the image plate within ~1-min exposure time, the image plate was scanned, and the spectral information was transferred to a computer in ~1.6 min. Thus, the total recording time for a spectrum is ~2.6 min. Most of the capillaries were heated up to 450 °C at a heating rate of 2.4 °C/min.

To investigate structural changes in charged $Li_{1-x}Ni_{0.8}Co_{0.15}Al_{0.05}O_2$ cathodes during thermal decomposition, time-resolved XRD analysis was performed. Time-resolved XRD patterns for $Li_{0.67}Ni_{0.8}Co_{0.15}Al_{0.05}O_2$ in the absence and presence of electrolyte are seen in Figs. 6 and 7, when heated from 25 °C to 450 °C. The structure of the cathode materials with electrolyte show dramatic changes with increasing temperature compared to that of the cathode materials without electrolyte. In the absence of electrolyte, no structural changes are seen until about 280 °C. As shown in Fig. 6b, the intensity of the critical (003) peak remains unchanged until about 280 °C, indicating that Ni atoms are not displaced to the Li-atoms planes. In the

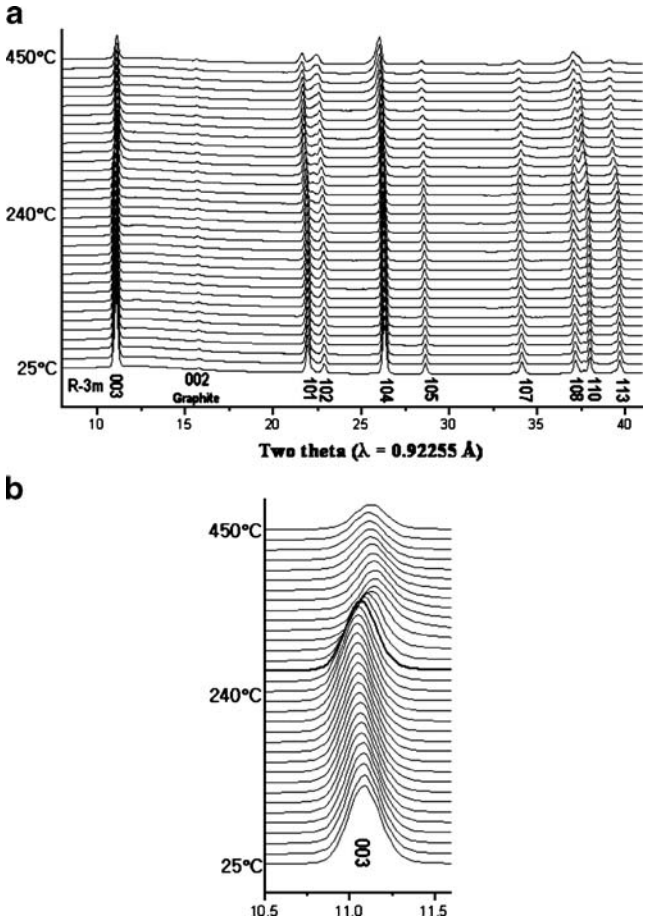

Fig. 6 **a** Time-resolved XRD patterns for $Li_{0.67}Ni_{0.8}Co_{0.15}Al_{0.05}O_2$ in the absence of electrolyte, when heated from 25 °C to 450 °C. **b** Magnified 003 peaks for **a**. Decomposition reaction starts at ~280 °C (*thick line*)

presence of electrolyte, decomposition reactions can be seen as low as 230 °C. The electrolyte accelerates thermal decomposition of the charged cathode material. The presence of the electrolyte changes the paths of the structural changes and lowers the temperatures for onset of the reactions. When subsequently heated at higher temperature, the disordered spinel structure converts to NiO-like rock salt structure. These decomposition processes involve oxygen release with exothermic reactions. XRD patterns for $Li_{0.67}Ni_{0.8}Co_{0.15}Al_{0.05}O_2$ in the presence and absence of electrolyte do not show clear evidence for the spinel phase during heating. For the sample with electrolyte, the number of the peaks decreased considerably after heating at 450 °C, as shown in Fig. 7. The XRD pattern at 450 °C is similar to the NiO structure and can be indexed assuming a cubic cell with a space group of Fm3m. Another interesting observation in the XRD pattern for the sample with electrolyte heated at above 400 °C is the formation of Li_2CO_3, suggesting that at low states of charge ($x<0.5$), the reaction of $Li_{1-x}Ni_{0.8}Co_{0.15}Al_{0.05}O_2$ with the electrolyte at elevated temperature forms NiO and Li_2CO_3. In the presence of electrolyte, the solvent acts as a reducing agent, and also, lithium extracted from the structure reacts with the solvent resulting in the formation of Li_2CO_3.

Figure 8a shows time-resolved XRD patterns for $Li_{0.27}Ni_{0.8}Co_{0.15}Al_{0.05}O_2$ in the presence of electrolyte, when heated from 25 °C to 450 °C. Decomposition of the layered structure starts at about 200 °C. In the interval between 200 °C and 250 °C, the coalescence of the (108) and (110) peaks in the layered structure is observed, suggesting the formation of a disordered spinel phase. Based on a 2×2×2 cubic rock salt lattice, this merged peak corresponds to the (440) peak in the cubic structure with space group Fd3m. The evolution of the (220) diffraction line also confirms the formation of the spinel phase (Fig. 8b). As can be seen in Fig. 8b, in addition to the well-defined peaks of the spinel structure, broad shoulders to the left of the spinel (400) and (440) peaks are also seen. These broad shoulders clearly indicate the presence of a second phase. We ascribe these shoulders to the nucleation of an additional phase. From the systematic growth of this minority phase (on further heating the sample), we can easily identify this phase to be the precursor to the final well-defined NiO-like (rocksalt) structure that is obtained. Figure 8c shows an expanded view of Fig. 8a in the temperature range between 270 °C and 302 °C. The broad peaks around the spinel (400) and (440) peaks transform into the relatively sharp (200) and (220) peaks of the NiO-

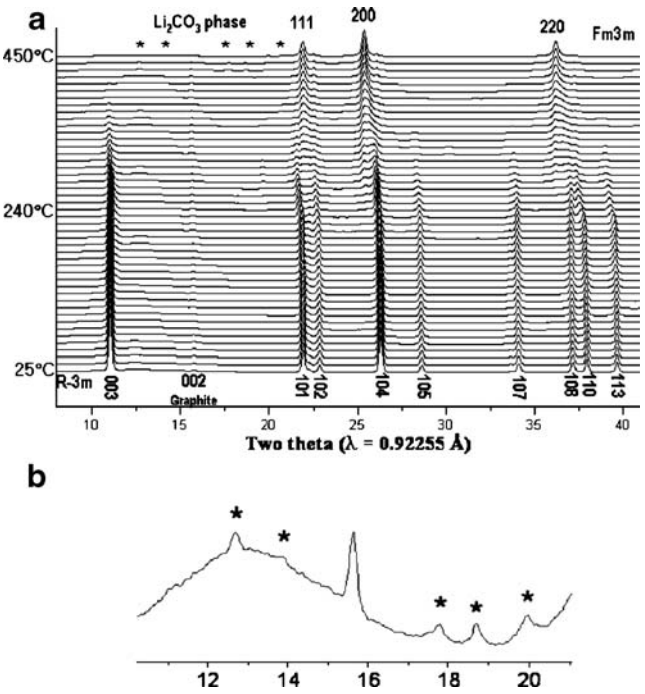

Fig. 7 **a** Time-resolved XRD patterns for $Li_{0.67}Ni_{0.8}Co_{0.15}Al_{0.05}O_2$ in the presence of electrolyte when heated from 25 °C to 450 °C. **b** Magnified XRD pattern at 450°C in **a**. *Asterisk* Formation of Li_2CO_3 phase

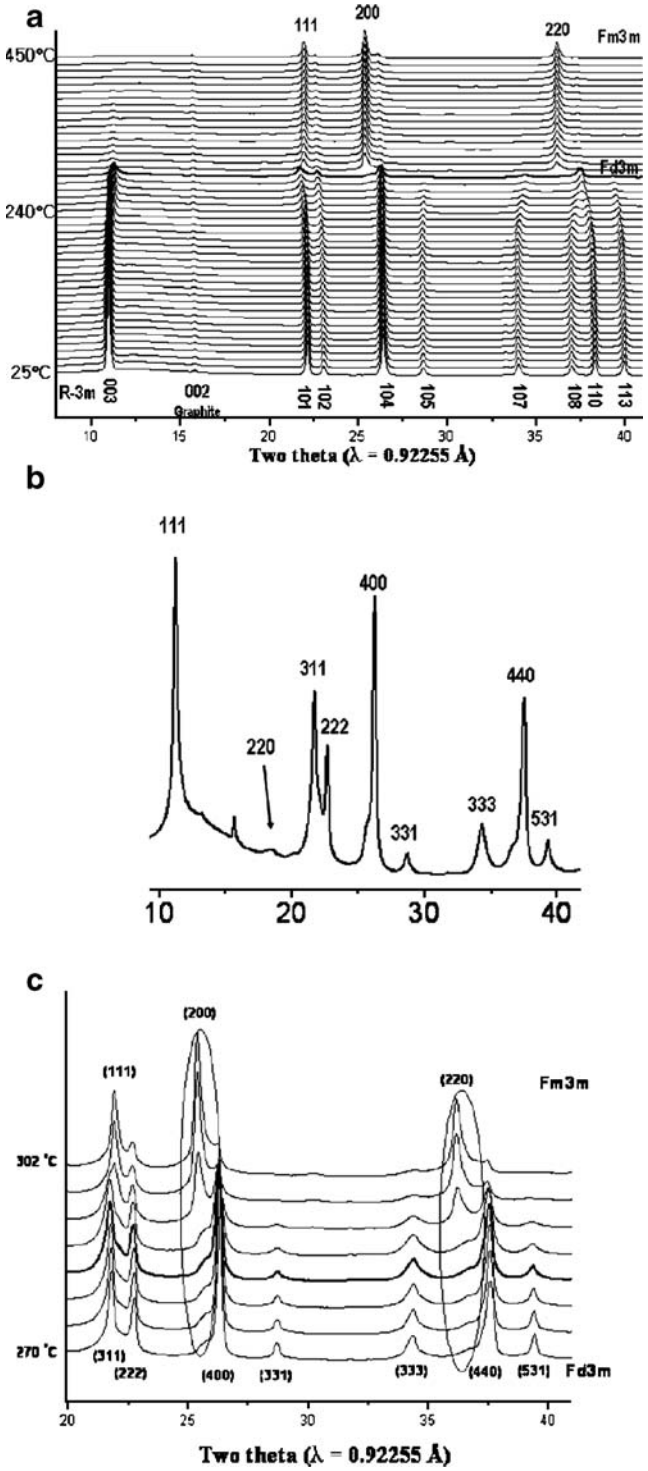

Fig. 8 **a** Time-resolved XRD patterns for $Li_{0.27}Ni_{0.8}Co_{0.15}Al_{0.05}O_2$ in the presence of electrolyte when heated from 25 °C to 450 °C (*thick line*: **b**). **b** Time-resolved XRD pattern for $Li_{0.27}Ni_{0.8}Co_{0.15}Al_{0.05}O_2$ at 280 °C. This is an expanded view of the thick line in **a**. The shoulders around the spinel (400) and (440) peaks indicate the presence of an additional phase. **c** Magnified XRD patterns in the temperature range between 270 °C and 302 °C in **a** (*thick line*: **b**)

like structure at the expense of the disordered spinel phase. Above 290 °C, a rock salt structure is observed, consistent with the formation of NiO-like phase. The disordered spinel phase transforms progressively to the NiO-like phase as the temperature increases. During the conversion from a spinel to a rock salt phase, both lithium and nickel ions move randomly to other layers. Therefore, the resulting rock salt phase has a unit cell with an axis of a half for the spinel phase. The transformation of the spinel phase to NiO-like rock salt phase is almost completed at the end of heating. The resulting peaks could be indexed, assuming a cubic cell with a space group of Fm3m.

In summary, at low states of charge ($x<0.5$), the reaction of $Li_{1-x}Ni_{0.8}Co_{0.15}Al_{0.05}O_2$ with the electrolyte at elevated temperature form NiO and Li_2CO_3. The solvent acts as a reducing agent, and also lithium is extracted from the structure and reacts with the solvent, resulting in the formation of Li_2CO_3. At high states of charge ($x>0.5$), the $Li_{1-x}Ni_{0.8}Co_{0.15}Al_{0.05}O_2$ cathode first converts from a layered structure to a disordered spinel structure, with the temperature of conversion decreasing with increased state of charge. The disordered spinel phase transforms to the NiO-like phase as the temperature increases.

Nonresonant inelastic X-ray scattering (NRIXS): a new technique for in situ NRIXS studies of the lithiation/delithiation process in Li-ion batteries

NRIXS is somewhat analogous to visible Raman spectroscopy. IXS studies require an intense X-ray beam with a typical incident flux of $\sim 5\times10^{12}$ s^{-1}. The typical incident photon energy is ~10 keV. The penetration length of ~10 keV X-rays in LiC_6 is well over 2 mm, ensuring a truly bulk-sensitive measurement. IXS requires the use of third generation light source. So far, there are three of these: the APS at Argonne, the European Synchrotron Radiation Facility at Grenoble, and the Spring-8, Japanese Synchrotron Radiation Research Institute at Nishi-Harima.

Recently, Balasubramanian et al. [12] used IXS to study the details of the charge transfer between the Li intercalant and the graphite host in LiC_6. This has been a subject of contention. This situation is largely due to the extreme sensitivity of Li-intercalated graphite to oxygen (and other contaminants) together with the surface sensitivity of many of the relevant spectroscopic techniques. By using IXS, these workers were able to overcome these problems through the use of hard X-ray NIXS, focusing on the contribution to IXS from the Li and C 1s initial states. This type of IXS is unique among the relevant core-shell spectroscopies in having intrinsic bulk sensitivity and easy compatibility with a wide range of sample environments. To analyze the IXS data, it is necessary to remove the valence Compton contribution to the total IXS signal by the subtraction of a smooth background.

In Fig. 9, we show the Li 1s contribution to the IXS cross section for Li metal, LiF (single crystal, Alpha Aesar), chemically prepared LiC_6 with **q** approximately parallel to $\hat{e}$, chemically prepared LiC_6, with **q** spanning 10°–30° from the basal plane, the unwashed electrochemically lithiated LiC_6 sample, and the corresponding washed sample. Interspersed in Fig. 9 (d) and (f) are ab initio calculations, as labeled.

The dashed vertical line in Fig. 9 (54.8 eV) shows the position of the absorption edge of Li metal. Allowing for differences in experimental details, the Li metal results are in good agreement with prior measurements of IXS. However, the Li metal measurements are in disagreement with the electron energy loss spectroscopy (EELS) measurements of Hightower et al. [13], where the midpoint of the leading edge of the spectrum is shifted upward by ~2 eV with respect to the present results. The results on the second reference material, LiF, are in good agreement with prior measurements by EELS and XAFS.

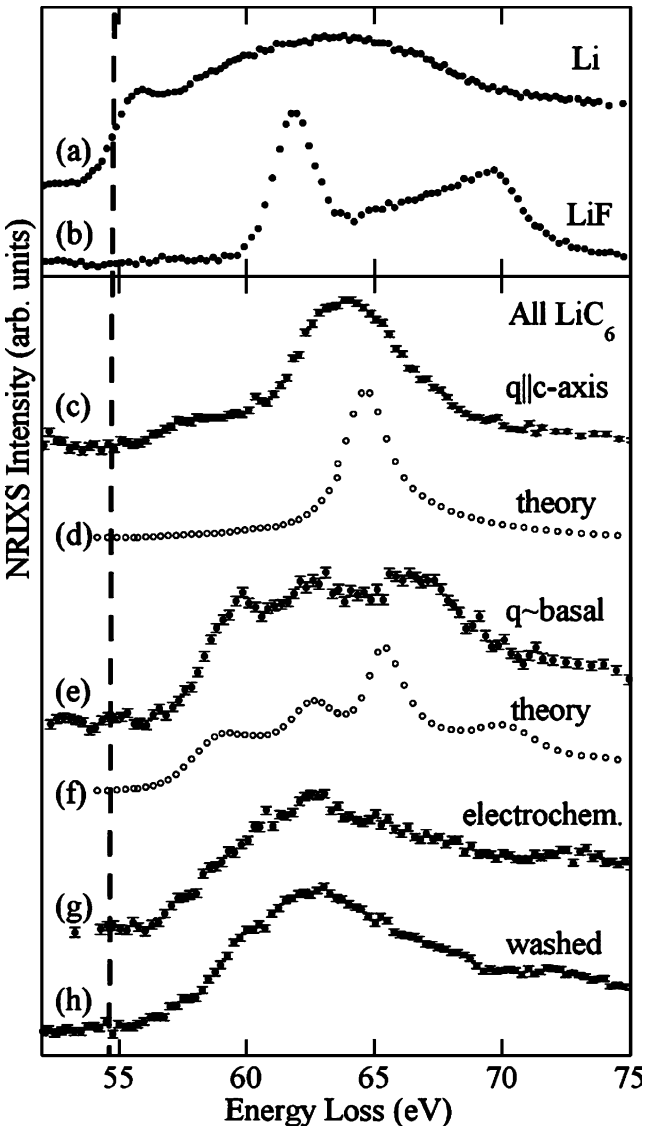

Fig. 9 Li 1s IXS intensity for several materials. (*a*) Li metal, with q=0.8 Å^{-1}. (*b*) LiF, with q=0.8 Å^{-1}. (*c*) Chemically prepared LiC_6, with **q** approximately parallel to $\hat{e}$ and having q=0.8 Å^{-1}. (*d*) Ab initio calculation for the same conditions as in (*c*). (*e*) Chemically prepared LiC_6, with **q** spanning 10°–30° from the basal plane and having an average q=9 Å^{-1}. (*f*) Ab initio calculation for q parallel to basal plane for q=10.4 Å^{-1}. (*g*) Electrochemically prepared LiC_6, with q=0.8 Å^{-1}. (*h*) Electrochemically prepared LiC_6 washed with dry acetonitrile and having q=0.8 Å^{-1}

In summary, the authors found overwhelming evidence in favor of a ~2 eV chemical shift in the Li 1s edge position of LiC_6 with respect to Li metal, for both chemical and electrochemical sample preparations. The observed IXS from the C 1s initial state shows a modest decrease in the σ threshold, but no change in the position of the π^* resonance in LiC_6 with respect to graphite. This behavior is understood as a consequence of charge transfer from the Li intercalant to the π bands of the graphitic sheets and the concomitant increase in the C–C distance. This study demonstrates the ready compatibility of IXS with electrochemically prepared materials, especially as regards the insensitivity of IXS to residual electrolyte. This is an important experimental proof of principal for future in situ IXS studies of the lithiation/delithiation process in Li-ion batteries.

Synchrotron X-ray reflectometry studies on two-dimensional model lithium battery cathodes

Twenty years ago, the synchrotron X-ray reflectivity method was used to detect the electrode surface of single crystal metal electrodes in contact with the electrolyte. The technique was used with great effect to study surface relaxation, surface reconstruction, and underpotential deposited layers [14–18]. Recently, a large group at the Japanese Spring-8 synchrotron has applied the synchrotron X-ray reflectivity method to the study of lithium metal oxide cathodes [19–21]. These three publications cover X-ray reflectometry studies on $LiCoO_2$, $LiMn_2O_4$, and $LiNi_{0.8}Co_{0.2}O_2$. To get useful data that can be interpreted, one must have an ideal electrode system with highly oriented model electrodes with an electrode surface that is flat and with a roughness that is no more than ~1 nm.

$LiCoO_2$ $LiCoO_2$ films were grown using a KrF excimer laser with a wavelength of 248 nm under O_2 and a pulsed laser deposition (PLD) apparatus, PLD 3000 (PVD products). The substrates used were single crystals of Nb doped $SrTiO_3$ (10 mm×10 mm×5 mm size). The conductivity of the substrate was 5.28×10^{-3} Ω cm at room temperature. The orientations of the substrate crystals were (111), (110), and (100) for $SrTiO_3$. The targets for the PLD process were synthesized by sintering starting materials at high temper-

atures. Li_2CO_3 and Co_3O_4 were used for the starting materials. The target had an excess lithium composition (Li/Co=1.0–1.3) to compensate lithium loss during the PLD process. The deposition rate of the film was about 0.3 nm min^{-1}, and the film thickness was 5–20 nm depending on the duration of the deposition. The use of higher O_2 pressure and lower substrate temperature reduced the cation mixing at the 3*a* and 3*b* sites, and the film showed more than 90% ordering at these sites. Epitaxial growth was confirmed for all the substrates used. Ex situ X-ray reflectivity spectra of the as-prepared (110) and (003) could be best fitted to a three-layer model composed of the $SrTiO_3$ substrate, the $LiCoO_2$ film, and a surface layer. The surface was covered by an impurity phase with low density, which is most likely a lithium-containing phase, such as lithium carbonate or lithium hydroxide. Upon immersion in the electrolyte, the surface layer dissolves. Ex situ and in situ X-ray reflectivity on the washed electrodes indicated that a new surface electrode interface (SEI) phase was observed only on the intercalation active plane, $LiCoO_2$ (110). This SEI phase was observed from the very beginning of the washing process. However, the $LiCoO_2$ (003) surface remained unchanged. The electrode surface of the (110) was affected by the intercalation reaction, and the surface roughness of the (110) plane increased. The electrochemical characterization of these films revealed that the $LiCoO_2$ (003) had only a limited capacity, while the $LiCoO_2$ (110) plane had a reversible electrode reaction, which is consistent with the layered structure of $LiCoO_2$ that permits active intercalation on the sites situated on the edge planes of the 2D layered structure.

$LiMn_2O_4$ The $LiMn_2O_4$ films showed (111), (110), and (100) orientations on the $SrTiO_3$ (111), (110), and (100) substrates, respectively. The films with (111), (110), and (100) orientations showed good cycling characteristics, with no orientation dependence until five cycles. These results were consistent with the three-dimensional ionic diffusion in the framework structure of $LiMn_2O_4$. Ex situ X-ray reflectivity spectra of the as-prepared (111), (110), and (100) $LiMn_2O_4$ layers could be best fitted to a three-layer model composed of the $SrTiO_3$ substrate, the $LiMn_2O_4$ film, and a surface layer. The surface layers had similar properties to those found for as-prepared $LiCoO_2$. There was no lattice-plane dependence of the impurity layer formation. These top surface layers also dissolved in the electrolyte. Ex situ and in situ X-ray reflectivity measurements on the washed electrodes indicated that a new SEI phase was observed only on the (111) plane. The data could be fitted with a three-layer model. The results indicated that surface layer had a density of 3.9 g cm^{-3} and a thickness of 2.14 nm. The density is somewhat lower than the 4.3 g cm^{-3} for $LiMn_2O_4$. This may be due to a defect layer formed by a reaction between the electrolyte and $LiMn_2O_4$. This type of layer was not observed on the $LiMn_2O_4$ (110) and (100) films. However, in situ XRR measurements detected a decrease in the film thickness of $LiMn_2O_4$ (110) during the first charging process. This could be due to the dissolution of the film due to the disproportionation reaction of the unstable Mn^{3+} to Mn^{2+} and Mn^{4+} at the surface. The in situ XRR measurements indicated no changes in the thickness of the $LiMn_2O_4$ (111) film during charge.

$LiNi_{0.8}Co_{0.2}O_2$ The as-prepared $LiNi_{0.8}Co_{0.2}O_2$ had an impurity phase on the surfaces. The impurity phase on the $LiNi_{0.8}Co_{0.2}O_2$ (110) film was thicker (2.2 nm) than that on the $LiNi_{0.8}Co_{0.2}O_2$ (003) film (1.0 nm). The $LiNi_{0.8}Co_{0.2}O_2$ films have a 2D transition metal layer parallel and perpendicular to the substrates depending on the substrate orientation. The electrochemical properties of these films showed anisotropic properties depending on the film orientations. The surface reaction with lithium proceeded on the $LiNi_{0.8}Co_{0.2}O_2$ (110) plane, where the lithium layer is perpendicular to the interface. This is consistent with the charge–discharge behavior of the (110) and (003) films. X-ray reflectivity studies indicated the formation of a SEI phase on the (110) lattice plane when the electrode was soaked in the electrolyte. No SEI layer was formed on the (003) plane. However, there was an increase in surface roughness when a potential was applied.

The combination of X-ray reflectometry with epitaxial thin film electrodes is a promising technique for the elucidation of interfacial reactions at the electrode/electrolyte interface.

Acknowledgment Brookhaven National Laboratory is supported by the U.S. Department of Energy under Contract No. DE-AC02-98CH10886.

References

1. Habib MA, Bockris JO'M (1984) J Electroanal Chem 180:287 doi:10.1016/0368-1874(84)83587-X
2. Sayers DE, Stern EA, Lytle FW (1971) Phys Rev Lett 27:1204 doi:10.1103/PhysRevLett.27.1204
3. Yoon W-S, Grey CP, Balasubramanian M, Yang X-Q, Fischer DA, McBreen J (2004) Electrochem Solid-State Lett 7:A53 doi:10.1149/1.1643592
4. Yoon W-S, Balasubramanian M, Chung KY, Yang X-Q, McBreen J, Grey CP, Fischer DA (2005) J Am Chem Soc 127:17479 doi:10.1021/ja0530568
5. Yoon W-S, Paik Y, Yang X-Q, Balasubramanian M, McBreen J, Grey CP (2002) Electrochem Solid-State Lett 5:A263 doi:10.1149/1.1513001
6. Balasubramanian M, McBreen J, Davidson IJ, Whitfield PS, Kargina I (2002) J Electrochem Soc 149:A176 doi:10.1149/1.1431962
7. Ceder G, Chiang Y-M, Sadoway DR, Aydinol MK, Jang Y-I, Huang B (1998) Nature 392:694 doi:10.1038/33647

8. Yoon W-S, Kim K-B, Kim M-G, Lee M-K, Shin H-J, Lee J-M, Lee J-S, Yo C-H (2002) J Phys Chem B 106:2526 doi:10.1021/jp013735e
9. Yoon W-S, Balasubramanian M, Yang X-Q, Fu Z, Fischer DA, McBreen J (2004) J Electrochem Soc 151:A246 doi:10.1149/1.1637896
10. Yoon W-S, Chung KY, McBreen J, Zaghib K, Yang X-Q (2004) Electrochem Solid-State Lett 9:A415 doi:10.1149/1.2216619
11. Yoon W-S, Balasubramanian M, Yang X-Q, McBreen J, Hanson J (2005) Electrochem Solid-State Lett 8:A83 doi:10.1149/1.1846714
12. Balasubramanian M, Johnson CS, Cross JO, Seidler GT, Fister TT, Stern EA, Hamner C, Mariager SO (2007) Appl Phys Lett 91:31904 doi:10.1063/1.2752755
13. Hightower A, Ahn CC, Fultz B, Rez P (2000) Appl Phys Lett 77:238 doi:10.1063/1.126936
14. Gibbs D, Ocko BM, Zehner DM, Mocherie SGJ (1988) Phys Rev B 38:7303 doi:10.1103/PhysRevB.38.7303
15. Ocko BM, Wang J (1990) Phys Rev Lett 68:1466 doi:10.1103/PhysRevLett.65.1466
16. Wang J, Robinson IK, Adzic RR (1998) Surf Sci 412–413:374 doi:10.1016/S0039-6028(98)00450-6
17. Samant MG, Toney MF, Borges GL, Blum L, Melroy OR (1988) Surf Sci Lett 193:L29 doi:10.1016/0039-6028(88)90314-7
18. Nagy Z, You H, Yonco RM, Melendres CA, Yun W, Maroni VA (1991) Electrochim Acta 36:209 doi:10.1016/0013-4686(91)85203-J
19. Hirayama M, Sonoyama N, Abe T, Minoura M, Ito M, Mori D, Yamada A, Kanno R, Terashima T, Takano M, Tamura K, Mizuki JI (2007) J Power Sources 168:493 doi:10.1016/j.jpowsour.2007.03.034
20. Hirayama M, Sonoyama N, Ito M, Minoura M, Mori D, Yamada A, Tamura K, Mizuki JI, Kanno R (2007) J Electrochem Soc 154:A1065 doi:10.1149/1.2778853
21. Hirayama M, Sakamoto K, Hiraide T, Mori D, Yamada A, Kanno R, Sonoyama N, Tamura K, Mizuki JI (2007) Electrochim Acta 53:871 doi:10.1016/j.electacta.2007.07.074